MOLECULAR AND CELLULAR BIOLOGY, Nov. 2002, p. 7744–7757 Vol. 22, No. 22
0270-7306/02/$04.00+0 DOI: 10.1128/MCB.22.22.7744–7757.2002

Complex Formation with Ypt11p, a rab-Type Small GTPase, Is Essential To Facilitate the Function of Myo2p, a Class V Myosin, in Mitochondrial Distribution in *Saccharomyces cerevisiae*

Takashi Itoh, Akiko Watabe, Akio Toh-e, and Yasushi Matsui*

Department of Biological Sciences, Graduate School of Science, University of Tokyo, Hongo, Tokyo 113-0033, Japan

Received 15 February 2002/Returned for modification 4 April 2002/Accepted 5 August 2002

We identified Ypt11p, a rab-type small GTPase, by its functional and two-hybrid interaction with Myo2p, a class V myosin of the budding yeast *Saccharomyces cerevisiae*. The tail domain of Myo2p was coimmunoprecipitated with Ypt11p, suggesting that Ypt11p forms a complex with Myo2p at its tail domain in vivo. Mutational analysis of *YPT11* suggests that Myo2p is a putative effector of Ypt11p. Deletion of *YPT11* induced partial delay of mitochondrial transmission to the bud, and overexpression of *YPT11* resulted in mitochondrial accumulation in the bud, indicating that Ypt11p acts positively on mitochondrial distribution toward the bud. We isolated two *myo2* mutants, *myo2-338* and *myo2-573*, which showed genetic interactions with *YPT11*. The *myo2-573* mutation, identified by a synthetic lethal interaction with *ypt11*-null, induced a defect in mitochondrial distribution toward the bud, indicating that Myo2p plays a crucial role in polarized distribution of mitochondria. The *myo2-338* mutation was identified as the mutation that abolished the effect of overexpressed *YPT11*, such as the Ypt11p-dependent accumulation of mitochondria in the bud, and the affinity of Myo2p for Ypt11p was reduced. These results indicate that complex formation of Ypt11p with Myo2p accelerates the function of Myo2p for mitochondrial distribution toward the bud.

Class V myosins, a crucial actin-based motor for organelle transport, are conserved from yeast to mammals and contain an N-terminal motor domain for interacting with actin structures and a C-terminal tail domain for the binding of cargo (5, 40). In the dilute mouse, which carries a defective class V myosin (myosin-Va), melanosomes localize in the central cell body of melanocytes instead of at the dendritic tip, indicating a failure of pigment transport (30). In the budding yeast, Myo2p is an essential class V myosin (1,574 amino acids) and localizes at the tip of growing buds (17, 23). Defects in Myo2p abolish polarized growth by disrupting the polarized delivery of secretory vesicles and lead to defects in vacuole inheritance, delivery of the late Golgi element, and transport of Kar9p for the orientation of mitotic spindles (13, 17, 31, 44). Therefore, Myo2p is essential for the polarized transport of organelles, such as secretory vesicles, vacuoles, late Golgi element, and Kar9p, along actin cables.

rab-type small GTPases participate in processes that underlie the targeting and fusion of membrane vesicles to their acceptor membrane. Small GTPases have three motifs for GTP binding and hydrolysis and have an effector domain between the first and second motifs for interaction with their effectors (2). Several putative effectors of rab-type small GTPases have been identified, and the diversity of their functions suggests that rab-type small GTPases play a more complex role than controlling the recognition of vesicles with membranes. It is reported that rab-type small GTPases interact with class V myosins. myosin-Vb colocalizes with and shows two-hybrid interaction with Rab11a, a rab-type small GTPase for the plasma membrane recycling system. N-terminal truncation of a myosin produces its dominant negative version, and the truncated myosin-Vb inhibits the recycling system, suggesting that Rab11a may play a role in docking the myosin motor to vesicles (20). myosin-Va, encoded by *dilute*, is required for pigment transport and is coimmunoprecipitated with Rab27a, a rab-type small GTPase (14). Dysfunction of Rab27a induces the pigment transport defect, which is similar to that observed in dilute cells. In ashen melanocytes, carrying defective Rab27a, myosin-Va fails to localize melanosomes (1, 25, 39, 41). Rab27a interacts with melanophilin, localized on melanosome membrane, and melanophilin interacts with myosin-Va (42). These observations suggest that Rab27a is involved in targeting myosin-Va to melanosome membranes. These studies of the mammalian cells show that activities of the rab-type small GTPase are required for myosin-V-driven organelle transport. However, the role of the complex formation between rab-type small GTPases and class V myosins has yet to be characterized.

We report here the identification of a rab-type small GTPase, Ypt11p, on the basis of its functional and physical interaction with Myo2p. This shows that the interaction between a rab-type small GTPase and a class V myosin is conserved from yeast to mammals. We identified that the pathway, involving both Myo2p and Ypt11p, affects mitochondrial distribution. Using genetic methods, highly developed in the yeast, we characterized the role of the complex formation between the class V myosin and rab-type small GTPase and revealed that the complex formation with Ypt11p is essential to facilitate the function of Myo2p in mitochondrial distribution.

* Corresponding author. Mailing address: Department of Biological Sciences, Graduate School of Science, University of Tokyo, Hongo, Tokyo 113-0033, Japan. Phone and fax: 81-3-5684-9420. E-mail: matsui@biol.s.u-tokyo.ac.jp.

MATERIALS AND METHODS

Media, plasmids, and strains. YPG and SCGal media were YPD, a rich medium, and synthetic complete (SC) medium (19), respectively, except that 2%

glucose was replaced with 2% galactose and 0.3% raffinose. SCraffinose is SC except that 2% glucose was replaced with 2% raffinose. All strains used were constructed in a YPH499 (33) background. For disruption of *YPT11* (*ypt11*Δ), a DNA fragment, containing the 700-bp 5′-noncoding region and the complete open reading frame (ORF) of *YPT11*, was amplified and inserted between the *Pst*I and *Xho*I sites of pBluescript KS(+) (Stratagene, La Jolla, Calif.) and the resultant plasmid was digested with *Hin*cII and ligated with a *Pvu*II fragment carrying *TRP1* to create pK001. The insert between the *Pst*I and *Xho*I sites was amplified by PCR and introduced into cells to create *ypt11*Δ cells. Wild-type strain YPH499 (33) was used to generate *ypt11*Δ strain yTO001. Using this construct, the DNA region encoding Ypt11p (amino acid residues 53 to 327) was replaced with the *TRP1* marker. To create YIpUGAL7-YPT11, a DNA fragment carrying the complete ORF of *YPT11* was amplified by PCR and inserted between the *Bgl*II and *Sal*I sites of YIpUGAL7, downstream from the *GAL7* promoter (24). YIpUGAL7-YPT11 digested with *Stu*I was integrated into the *ura3* locus. The DNA fragment containing the 700-bp 5′-noncoding region, complete ORF, and 579-bp 3′-noncoding region of *YPT11* was amplified by PCR and inserted between the *Sac*I and *Sal*I sites of pYO326, which is pRS306 (33) carrying the 2μm origin, to create pK008. To create *HA*-YPT11, which produces Ypt11p tagged with hemagglutinin (HA) at its N terminus under the control of the *YPT11* promoter, the *Pst*I-*Sal*I DNA fragment containing the 700-bp 5′-noncoding region of *YPT11*, the *Sal*I-*Xho*I DNA fragment encoding two copies of HA, and the *Xho*I fragment containing the complete *YPT11* ORF were prepared by PCR, ligated in frame, and inserted between the *Pst*I and *Xho*I sites of YCplac33, YEplac195, and YEplac112 (12) to create pK003, pK004, and p901EW-HA-YPT11, respectively. To create pK022 for production of Ypt11p tagged with green fluorescent protein (GFP) at its N terminus (GFP-Ypt11p) under the control of the *YPT11* promoter, the *Pst*I-*Xho*I DNA fragment containing the 700-bp 5′-noncoding region of *YPT11*, the *Sal*I-*Bam*HI DNA fragment encoding GFP, and the *Bgl*II-*Bgl*II fragment containing the complete *YPT11* ORF were prepared by PCR, ligated in frame, and inserted between the *Pst*I and *Bam*HI sites of YEplac195 (12). HA-Ypt11p and GFP-Ypt11p are functional because introduction of pK004 or pK022 suppressed Ts^- of *myo2-66* cells (data not shown). To create pK002 for production of GFP-tagged Ypt11p, the DNA fragment carrying the complete *YPT11* ORF was amplified and inserted in frame downstream of the GFP ORF on YEpGAL1, a high-copy-number plasmid carrying the *URA3* marker and the GFP ORF under the control of the *GAL1* promoter. To create plasmids for the GFP-tagged C-terminal tail domain of Myo2p (plasmid pGAL1-GFP-MYO2), the DNA fragment carrying the *MYO2* ORF (from codon 1031 to the stop codon) was amplified and inserted in frame downstream of the coding sequence for GFP-tag on YEpGAL1-GFP, a high-copy-number plasmid carrying the *URA3* marker and the sequence for GFP-tag under the control of the *GAL1* promoter. To observe the cellular localization of Myo2p, we modified the *MYO2* locus to produce Myo2p, tagged at its C terminus with GFP, under the control of the promoter. To produce the change, the DNA fragments carrying the ORF of *MYO2* or mutant *myo2* (from codons 1105 to 1574) were amplified and inserted in frame upstream of the *GFP* ORF for GFP-tag on an integration plasmid and the resulting plasmids were digested with *Stu*I and integrated into the *MYO2* locus to replace those of the GFP-tagged version. To create two-hybrid constructs of Myo2p, DNA fragments carrying the ORF (from codon 1031 to the stop codon) of *MYO2* (for pK016), *myo2-338* (for pK017), and *myo2-573* (for pK018) were amplified and introduced into pGAD-C1 (15) in frame. The DNA fragment carrying the *MYO2* ORF (from codon 1031 to the stop codon) and the DNA fragment carrying the *YPT11* ORF (for amino acid residues 1 to 352, lacking the C-terminal C-C motif, the modification site with an isoprenoid moiety) were introduced in frame into pGBDU-C1 (15) to create pK005 and pK027, respectively. pK027 was used for the two-hybrid screening against a yeast genomic library, based on the pGAD vector (15), and the *YPT11* clone, designated pK521, which contained the 156-bp 5′-noncoding region and ORF (encoding amino acid residues 1 to 305) of *YPT11* and thus encodes a 52-amino-acid spacer sequence between the *trans*-activator domain and Ypt11p, was isolated. Strain PJ69-4A (15) was used for the two-hybrid analysis. To create plasmids containing $ypt11^{G40D}$ or $ypt11^{1144N}$, DNA fragments encoding N-terminal Ypt11p and C-terminal Ypt11p were amplified individually by PCR using primers for amplification of *YPT11* ORF and divergent primers designed for the substitutions, 5′-TTGGAGACGCAAACGTCGA TAAGACAGCTA and 5′-CTTCCCGACGTTTGCGTCTCCAATTAGC for $ypt11^{G40D}$ and 5′-CGTCTTGATATCTATTCCGTTAGTACTTCT and 5′-GG AATAGATATCAAGACGAACTTGGTC for $ypt11^{1144N}$, digested with *Drd*I for $ypt11^{G40D}$ or *Eco*RV for $ypt11^{1144N}$, and ligated. The resulting fragments were digested with *Bst*EII, and the *Bst*EII fragments replaced the corresponding fragment in pK002, pK022, p901EW-HA-YPT11, and pK027 to create mutant versions of these constructs. To create plasmids for $ypt11^{V246D}$, the DNA fragment containing the 700-bp 5′-noncoding region and the region encoding N-terminal Ypt11p and the DNA fragment containing the region encoding the residual C-terminal Ypt11p and the 579-bp 3′-noncoding region of *YPT11* were amplified individually by PCR using primers for amplification of the region encompassing the *YPT11* gene and divergent primers designed for the substitutions: 5′-TGATGTTGATCAAATGGTTCAGGAAATGCA and 5′-ACCATTT GATCAACATCATAATGGGTTACCTG. The resultant fragments were digested with *Bcl*I, ligated, and inserted between the *Sac*I and *Sal*I sites of pRS306 (33). To create $ypt11^{V246D}$ cells (strain YMY111), the resultant plasmid was digested with *Stu*I and introduced into *ypt11*Δ cells (strain yTO001) to be integrated into the *ura3* locus.

For Kar9p tagged with GFP at the C terminus, the DNA fragment for 800 bp of the 5′-noncoding region and ORF of *KAR9* was amplified with the primers 5′-GGGGGGGCATGCGTAATTGGTCCTCACGGC and 5′-GGGGGGGTC GACATAAGTTGGGGTTTTATC and digested with *Sal*I and *Sph*I. The resultant fragment was inserted between the *Sal*I and *Sph*I sites of the YEplac195-derived plasmid, which carries the DNA fragment encoding GFP on YEplac195 (12), to be ligated in frame with the GFP-encoding region and used for the observation of the Kar9p localization. For the observation of Sec2p localization, the DNA fragment encoding C-terminal Sec2p (amino acids 268 to 759) was amplified with the primers 5′-GGGGGGCTCGAGGCATCGGCTGGTTGG TTA and 5′-GGGGGGGGATCCTTGCTGTTCCTGGGCATCAT and digested with *Xho*I and *Bam*HI. The resultant fragment was inserted between the *Xho*I and *Bam*HI sites of the YIplac204-derived plasmid, which carries the DNA fragment encoding GFP on YIplac204 (12), to be ligated in frame with the GFP-encoding region. The resultant plasmid (YIp-SEC2-GFP) was digested with *Xba*I and introduced into cells for integration into the *SEC2* locus to produce Sec2p tagged with GFP at the C terminus instead of the wild-type Sec2p. pSMY1 is an isolate, containing *SMY1*, from the screening of a high-dose-suppressor of *myo2-66*.

Screening of a high-dose suppressor of *myo2-66*. *myo2-66* cells (strain YMK021 [18]) were transformed with a yeast genomic library based on YEp24 (7) at 25°C and then incubated at 30°C for 2 to 4 days to select viable colonies at the nonpermissive temperature. Plasmids were recovered from the colonies and reintroduced into *myo2-66* cells to test the suppressing activity.

Isolation of *myo2-338* and *myo2-573* mutants. We mutagenized the limited *MYO2* region, encoding the C-terminal tail domain (amino acid residues 827 to 1569), and created Ts^- mutant cells, as follows. DNA fragments carrying the *MYO2* ORF (from codon 703 to the stop codon) were amplified using mutagenic PCR (6) and introduced between the *Pst*I and *Xho*I sites of pRS304 (33) carrying *TRP1*. The resulting plasmids were digested with *Mlu*I and introduced into wild-type cells (strain YPH499 [33]) at 25°C to replace the 3′ half of *MYO2* (downstream from the *Mlu*I site, located between codons 824 and 826 of the *MYO2* ORF) with the mutagenized half. Growth of about 900 Trp^+ transformants at 37°C was tested, and 28 *myo2* mutants that showed a temperature-sensitive growth phenotype (Ts^-) were isolated. The Ts^- transformants were crossed with *ypt11*Δ cells and subjected to tetrad analysis to examine both synthetic defects with *ypt11*Δ and cosegregation of Ts^- and Trp^+. One mutant (*myo2-573*) showed a synthetic growth defect with *ypt11*Δ. pK002 was introduced into the Ts^- cells for overexpression of *YPT11* in galactose-containing media, and transformants were streaked on SCGal plates lacking uracil and tryptophan. One mutant (*myo2-338*) grew on the plate. DNA fragments carrying the *myo2* ORF (from codon 673 to the stop codon) were amplified by PCR using the genome DNA of the mutants as a template and introduced into pRS304 to create plasmids to produce the mutant *myo2* alleles (pK014 for *myo2-338* and pK015 for *myo2-573*). pK014 and pK015 were digested with *Mlu*I and introduced into wild-type cells (strain YPH499) to create *myo2-338* cells (strain yTO014) and *myo2-573* cells (strain yTO015), respectively. Mapping and sequence analysis revealed that *myo2-338* carried three mutations, changing Leu 1474 to Ser, Glu 1484 to Gly, and Asp 1511 to Gly, and that *myo2-573* carried six mutations, changing Val 1189 to Ala, Val 1288 to Gly, Lys 1500 to Met, Pro 1529 to Ser, Glu 1546 to Gly, and Lys 1559 to Arg.

Morphological observation. To visualize mitochondria, 2-(4-dimethylaminostyryl)-1-methylpyridinium iodide (DASPMI) was used as described by Miyakawa et al. (26) or a high-copy-number plasmid carrying the fragment encoding GFP fused with the *COX4* signal sequence under the control of the *ADH1* promoter was introduced into cells. The cells were cultured, harvested at early log phase, and used for experiments. Almost identical results were obtained using the two methods of visualization. Rhodamine-phalloidin staining of actin and indirect immunofluorescent staining were performed as described previously (18). Anti-HA mouse antibodies (16B12; BAbCo), anti-HA rat antibodies (Boehringer), anti-GFP mouse antibodies (Roche Diagnostics), Alexa 546-conjugated anti-rat immunoglobulin G (IgG) (Molecular Probes) and fluorescein isothiocyanate

(FITC)-conjugated anti-mouse IgG (ICN) were used. The FM4-64 staining method (38) was used for vacuole observation. 4′,6-Diamidino-2-phenylindole (DAPI) was used for DNA staining. Images were recorded by an Olympus IX70 instrument with a SENSYS III cooled charge-coupled device CCD camera using IP Lab software (Olympus Co., Tokyo, Japan).

Immunoprecipitation. Immunoprecipitation was carried out essentially as described previously (37). Cells, carrying plasmids for producing HA-tagged and GFP-tagged proteins, were cultured in SCraffinose medium lacking uracil and tryptophan and shifted into SCGal medium lacking uracil and tryptophan to induce the production of the tagged proteins at 25°C. At 2.5 h after the shift, the cells were harvested and disrupted with glass beads in lysis buffer (200 mM NaCl, 100 mM Tris-HCl [pH 7.5], 0.5% CHAPS, 1 mM EDTA, 5% glycerol, 0.5 mM dithiothreitol, protease inhibitors [antipain, leupeptin, pepstatin, and aprotinin]). The lysate was centrifuged at 2,400 × *g* for 10 min with a microcentrifuge, and the resultant supernatant was used as the cell lysate. In the cell lysate, both tagged Ypt11p and Myo2p were soluble, since almost all of both proteins in the cell lysate were recovered in the supernatant after centrifugation of the lysate at 100,000 × *g* for 1 h. The cell lysate (10 mg of protein/ml) was incubated with anti-HA antibodies (16B12) at 4°C for 2 h and then precipitated using protein A-Sepharose (Amerhsam Pharmacia Biotech.). The precipitates were analyzed by Western blotting. Anti-HA antibodies (12CA5) and anti-GFP antibodies (Boehringer) were used for the detection.

RESULTS

Isolation of Ypt11p by two-hybrid and functional interaction with Myo2p. To investigate Myo2p function, we searched for a gene that acts as a high-dose suppressor of the *myo2-66* defect and also searched for the protein that interacts with the C-terminal tail domain of Myo2p, using a two-hybrid method (15). In both screenings, we found *YNL304w*, a gene that encodes a rab-type small GTPase of 356 amino acids, but its function has not been reported. It was designated *YPT11*, in accordance with a recent proposal (21).

The introduction of *YPT11* via a high-copy-number plasmid suppressed the temperature-sensitive growth phenotype by the *myo2-66* mutation, causing substitution at position 511 in the motor domain of Myo2p (Fig. 1A). This suggests that Ypt11p is functionally related to Myo2p. In the two-hybrid screening using the C-terminal tail domain of Myo2p (amino acid residues 1131 to 1574) as bait, we isolated a DNA fragment encoding Ypt11p (amino acid residues 1 to 305), suggesting a physical interaction between Ypt11p and Myo2p. To examine complex formation between Ypt11p and the tail domain of Myo2p in vivo, we used an immunoprecipitation assay. As shown in Fig. 1B, the C-terminal tail domain of Myo2p was coimmunoprecipitated with HA-tagged Ypt11p. As a control, we examined mutants Ypt11p, Ypt11p^{1144N}, and Ypt11p^{G40D}, which failed to show the two-hybrid interaction with Myo2p (see below). A reduced amount of Myo2p was coprecipitated with Ypt11p^{G40D}, and no detectable amount of Myo2p was coprecipitated with Ypt11p^{1144N}. Therefore, these results indicate that Ypt11p formed a complex with the C-terminal tail domain of Myo2p in the cell, as suggested by the two-hybrid analysis.

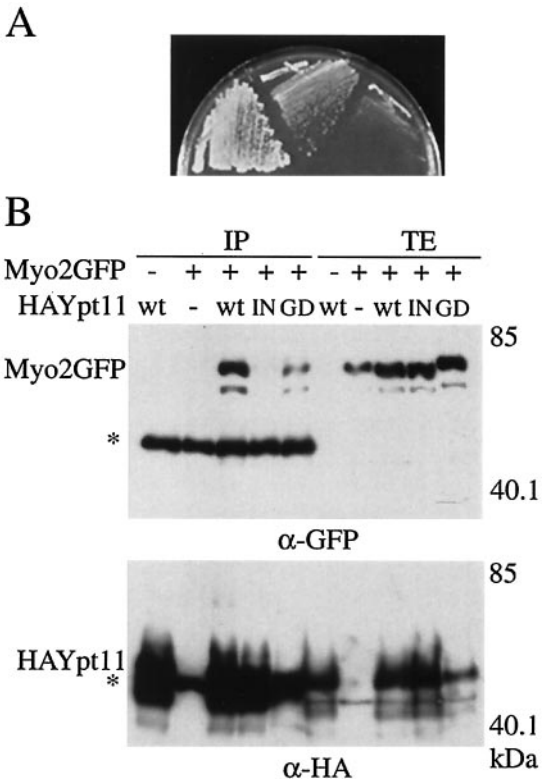

FIG. 1. Functional and physical interactions between Myo2p and Ypt11p. (A) Suppression of *myo2-66* with a high dose of *YPT11*. *myo2-66* cells (strain YMK021) with *MYO2* on a low-copy-number plasmid (left), with a high-copy-number plasmid carrying *YPT11* (pK008, middle), or with a control vector (pYO326, right) were streaked on an SC plate lacking uracil and incubated at 30°C for 3 days. (B) Complex formation between Ypt11p and the C-terminal tail domain of Myo2p. *ypt11*Δ cells (strain yTO001), carrying pGAL1-Myo2 for producing the GFP-tagged C-terminal tail domain of Myo2p (Myo2GFP +), YEpGAL1 as a control vector (Myo2GFP −) with the indicated plasmid for HA-tagged Ypt11p (wt, HA-tagged Ypt11p from p901EW-HA-YPT11; IN, HA-tagged Ypt11^{1144N}p from p901EW-HA-YPT11^{1144N}; GD, HA-tagged Ypt11^{G40D}p from p901EW-HA-YPT11^{G40D}), or control vector p901EW (−), plasmid YEplac112 (12) with an insert for the HA-tag, were disrupted, and the resulting cell extracts were immunoprecipitated with anti-HA antibodies. The total cell lysate (TE; 1 μg of protein from the cell lysate) and immunoprecipitate (IP; precipitate from 1.6 mg of protein from the cell lysate) were analyzed by Western blotting using anti-GFP antibodies (top) and anti-HA antibodies (bottom). The migration positions of GFP-tagged Myo2p and HA-tagged Ypt11p are indicated by Myo2p-GFP and HA-Ypt11p, respectively. Asterisks indicate the migration positions of IgG. Numbers at the right indicate the molecular mass of the protein marker in kilodaltons. About 0.06% of the Myo2p tail in the lysate was coimmunoprecipitated with the wild-type HA-Ypt11p, judging from the figure. Ypt11p migrated more slowly in the sodium dodecyl sulfate gel than expected from its calculated molecular mass. Bacterially produced Ypt11p also migrated as slowly as Ypt11p in the lysate, suggesting that the slow migration of Ypt11p is due to its protein nature rather than a consequence of posttranslational modification.

Cellular localization of Ypt11p and *YPT11*-overexpressing phenotypes. Using HA-tagged Ypt11p, we determined the cellular localization of Ypt11p. When *YPT11* was replaced with the HA-tagged version of *YPT11* on a low-copy-number plasmid, the signal of HA-tagged Ypt11p was detected in the bud of the small-budded cells, although the signal was very faint (Fig. 2, top left). When HA-tagged Ypt11p was produced from a high-copy-number plasmid, the signal became clearer (Fig. 2, top right). Ypt11p was concentrated at the site of bud emergence, at the bud tip of the growing bud, and at the bud neck during the M phase, judging from the actin organization of the cells (Fig. 2, bottom). Double immunofluorescent staining of Myo2p and Ypt11p revealed that Myo2p and Ypt11p were colocalized during the cell cycle (Fig. 2, middle).

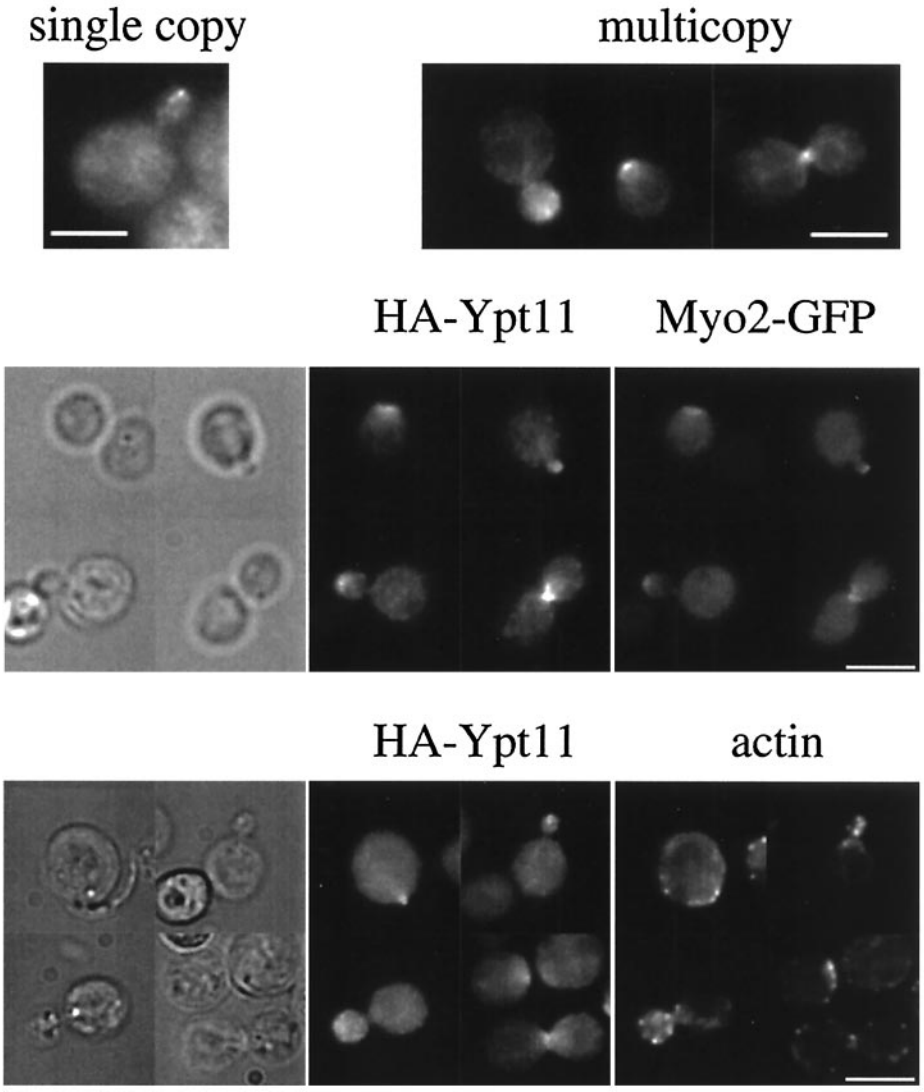

FIG. 2. Cellular localization of Ypt11p. (Top) *ypt11*Δ cells (strain yTO001) with pK003 (single copy), a low-copy-number plasmid carrying *HA-YPT11*, which produces Ypt11p tagged with HA at its N terminus under the control of the *YPT11* promoter, or with pK004 (multicopy), a high-copy-number plasmid carrying *HA-YPT11*, were grown in SC medium lacking uracil, fixed, and stained by the indirect-immunofluorescence method using anti-HA mouse antibodies (16B12) and FITC-conjugated anti-mouse IgG. (Middle) Wild-type cells (strain YPH499) with pK004 and a GFP-tagged version of *MYO2*, replacing the wild-type *MYO2* allele, were grown in SC medium lacking uracil, fixed, stained by the indirect-immunofluorescence method using anti-HA rat antibodies (HA-Ypt11) and anti-GFP mouse antibodies (Myo2-GFP), and visualized with Alexa 546-conjugated anti-rat IgG and FITC-conjugated anti-mouse IgG, respectively. Phase-contrast images are shown on the left. (Bottom) Wild-type cells (strain YPH499) with pK004 were grown in SC medium lacking uracil, fixed, and stained by rhodamine-phalloidin (actin) and the indirect immunofluorescence method using anti-HA mouse antibodies (16B12) and FITC-conjugated anti-mouse IgG (HA-Ypt11). Phase-contrast images are shown on the left. Bars, 5 μm.

Disruption of *YPT11* did not affect cell growth, cell morphology, organelles (including nuclei, vacuoles, and mitochondria), or the organization of actin cytoskeleton (data not shown). However, *YPT11* overexpression induced interesting phenotypes, such as inhibition of cell growth (Fig. 3A). Moreover, *YPT11*-overexpressing cells showed aberrant mitochondrial distribution (Fig. 3B). At 1 h after the induction of *YPT11* overexpression by the *GAL7* promoter using 2% galactose in the medium, mitochondria began to accumulate in the daughter bud. At 3 h after the induction, about 80% of cells with a middle-sized bud accumulated mitochondria in the bud and there were no more than two faint cables of mitochondria in the mother cells (Fig. 3B, right). At 8 h after the induction, most cells, independent of their mitochondrial content, became unbudded and ceased to grow, suggesting a defect in bud emergence (data not shown). In the absence of *YPT11* overexpression, mitochondria were detected in the mother cells as well as in the bud (Fig. 3B, left). We visualized mitochondria using DASPMI (26) and GFP, which was targeted into mitochondria via a *COX4* signal sequence, and both methods produced essentially the same results. In the *YPT11*-overexpressing cells, cell morphology, other organelles (vacuoles and

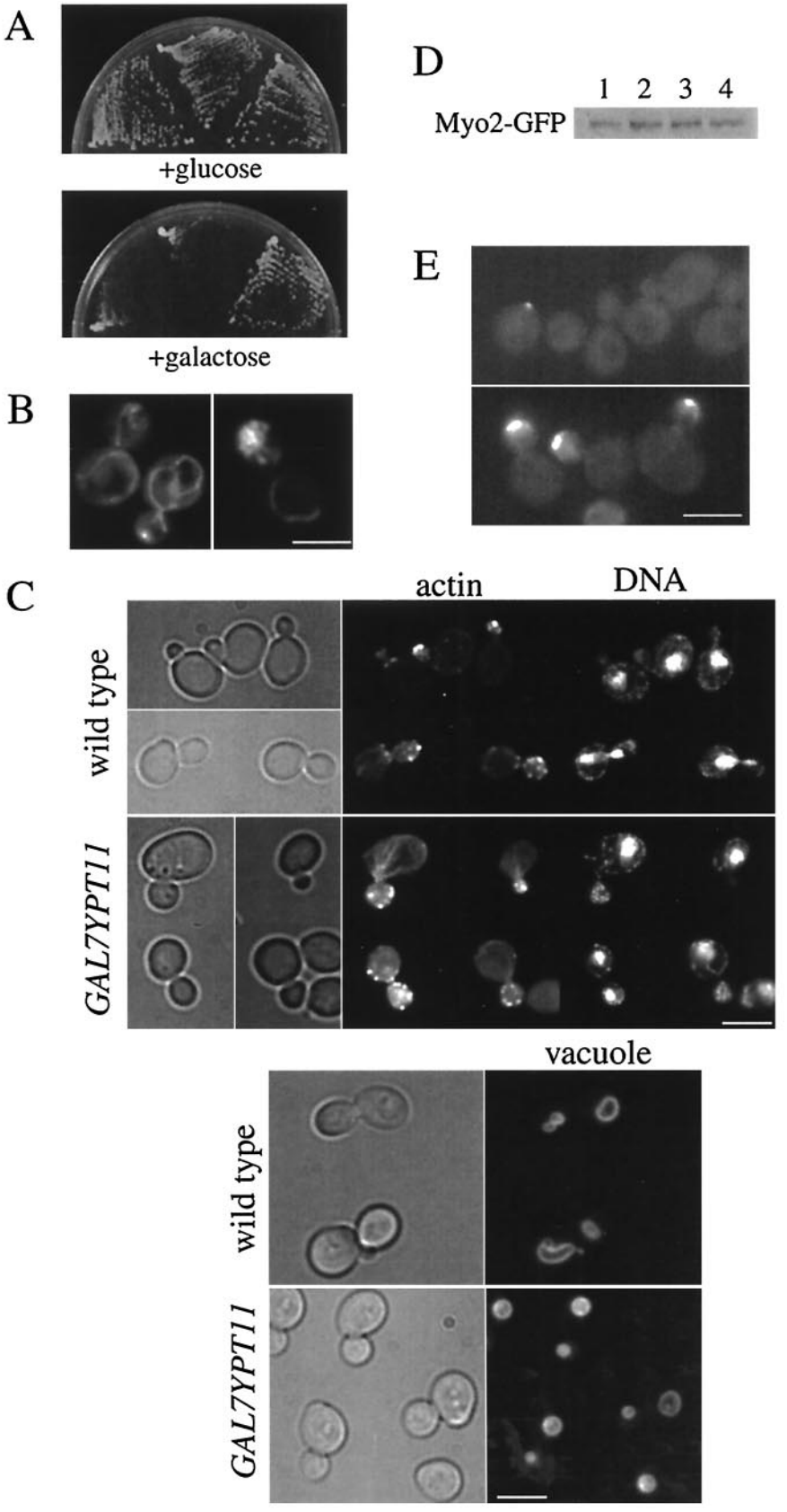
A
+glucose
+galactose
B
C
actin
DNA
wild type
GAL7YPT11
vacuole
wild type
GAL7YPT11
D
1 2 3 4
Myo2-GFP
E

nuclei), and organization of actin cytoskeleton were normal (Fig. 3C). The accumulation of mitochondria in the bud is not merely a consequence of growth inhibition by overproduction of a toxic protein, since we observed cells expressing a dominant inhibitory *CDC42, CDC42Val-12*, or *CDC42Ala-118* mutant (45) under the control of the *GAL7* promoter and found that the mitochondrial distribution of the cells was normal (data not shown). In addition, when 0.2% galactose was used in the medium for partial induction of *YPT11* overexpression, cells accumulated mitochondria in the bud although cell growth was not inhibited. Cellular amounts of Myo2p were not affected by overexpression of *YPT11* or by the carbon sources (Fig. 3D). Therefore, the asymmetric distribution of mitochondria suggests that Ypt11p acts positively and directly on the distribution of mitochondria to the bud. The phenotype of the reported mutants for mitochondrial distribution is the defect in mitochondrial transmission to the bud (43). Therefore, the phenotype, acceleration of mitochondrial distribution to the bud, is novel.

We examined the cellular localization of Myo2p in *YPT11*-overexpressing cells. In *YPT11*-overexpressing cells, Myo2p was detected at the cortex around the bud tip as a prominent signal in both small and middle-sized buds (Fig. 3E, bottom). In the absence of *YPT11* overexpression, Myo2p was detected clearly only at the bud tip in the small-budded cells and faintly in a middle-sized bud (Fig. 3E, top). These observations suggest that Ypt11p increases the Myo2p concentration in the bud.

Mitochondrial transmission of *ypt11*-deficient cells. At the early stage of bud formation, emerging buds often lack mitochondria, but most of the small buds, whose diameter becomes about 1.5-fold the diameter of bud neck, possess mitochondria (typical images of mitochondria in the small-budded cells are shown in Fig. 4, left). These observations indicate that mitochondria are transmitted to the small bud during bud growth rather than being transmitted exclusively at the beginning of bud emergence. Although disruption of *YPT11* did not affect mitochondrial distribution and morphology, Ypt11p can accelerate mitochondrial transmission to the bud. Therefore, we examined the effect of dysfunction of Ypt11p on the transmission of mitochondria at the early stage of bud formation.

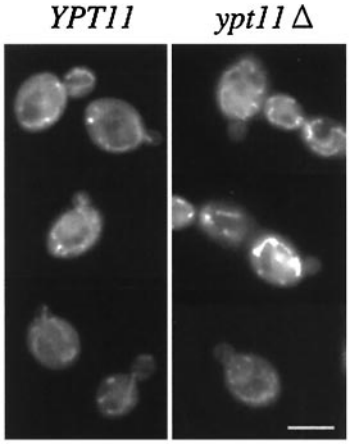

FIG. 4. Mitochondria in small-budded cells. Small-budded cells (wild-type diploid cells [left] and *ypt11*Δ/*ypt11*Δ homozygous diploid cells [right]) were stained with DASPMI. Typical wild-type cells possessing mitochondria in the bud and *ypt11*Δ cells lacking mitochondria in the bud are shown. Bar, 5 μm.

In the early-log-phase culture, about 90 and 85% of small-budded wild-type haploid cells and diploid cells, respectively, transmitted mitochondria into the small bud (Table 1). However, mitochondria were not detected in about 25 and 34% of the small buds of haploid *ypt11*Δ cells and homozygous diploid *ypt11*Δ/*ypt11*Δ cells, respectively (Table 1; typical images of the *ypt11*Δ small-budded cells lacking mitochondria in the bud are shown in Fig. 4, right). These results indicate that loss of Ypt11p causes a delay of mitochondrial transmission to the small bud. We examined this phenotype by using a putative conditional *ypt11* allele, $ypt11^{V246D}$. The $ypt11^{V246D}$ mutation, which replaces Val 246 of Ypt11p with Asp, corresponds to the mutations that convert rab-type GTPases to temperature sensitivity, such as *sec4-8* and *ypt1-A136D* (16). Small buds of $ypt11^{V246D}$ cells retained mitochondria to almost an equal ex-

FIG. 3. Phenotypes of *YPT11*-overexpressing cells. (A) Inhibition of cell growth with overexpressed *YPT11*. Two independent transformants of wild-type cells (strain YPH499) with YIpUGAL7-YPT11 (an integrated plasmid carrying *YPT11* under the control of the *GAL7* promoter [left and middle sectors]) and wild-type cells without YIpUGAL7-YPT11 (right sector) were streaked on a glucose-containing rich medium, YPD (left), or galactose-containing medium, YPG (right), and incubated at 30°C for 3 days. (B) Mitochondria in *YPT11*-overexpressing cells. Wild-type cells (strain YPH499) with (right) or without (left) YIpGAL7-YPT11 were cultured until early log phase in SCraffinose medium, shifted into SCGal medium for induction, incubated for 4 h at 25°C, and stained with DASPMI to visualize mitochondria. We estimated the level of overexpression by using HA-tagged versions of the *YPT11* constructs. About a 30-fold-increased amount of Ypt11p was detected in the cells by the overexpression with the *GAL7* promoter, compared with that in the cells carrying *YPT11* on a high-copy-number plasmid (pK004). (C) Actin, nuclei, and vacuole in *YPT11*-overexpressing cells. Wild-type cells (strain YPH499) without (wild type) or with (*GAL7YPT11*) YIpGAL7-YPT11 were cultured until early log phase in SCraffinose medium, shifted into SCGal medium for induction, and incubated for 2 h at 25°C. The cells were fixed and stained using rhodamine-phalloidin (actin) and DAPI for nuclei (DNA) or observed by FM4-64 staining (vacuole). Phase-contrast images are shown on the left. (D) Cellular amounts of Myo2p in *YPT11*-overexpressing cells. The *MYO2* locus of the wild-type cells (strain YPH499) was replaced with *MYO2* fused with GFP for producing Myo2p tagged at the C terminus with GFP under the control of its own promoter. The cells with YIpUGAL7-YPT11 for *YPT11* overexpression (lanes 2 and 4) or without the plasmid (lanes 1 and 3) were cultured until early log phase in SCraffinose medium (lanes 1 and 2), shifted into SCGal medium, and incubated for 2 h (lanes 3 and 4) at 25°C. The cells were harvested and disrupted with glass beads. The same amount of proteins in each cell lysate was analyzed by Western blotting using anti-GFP antibodies. (E) Cellular localization of Myo2p in *YPT11*-overexpressing cells. The *MYO2* locus of the wild-type cells (strain YPH499) was replaced with *MYO2* fused with GFP for producing Myo2p tagged at the C terminus with GFP under the control of its own promoter. The cells with YIpUGAL7-YPT11 for *YPT11* overexpression (bottom) or without the plasmid (top) were incubated in galactose-containing medium for 2 h. Both images were recorded under the same exposure conditions; under these conditions, the GFP-tagged Myo2p was hardly recorded in the cells without *YPT11* overexpression except for in small-budded cells. Bars, 5 μm.

TABLE 1. Percentages of small buds without mitochondria[a]

Genotype	Culture temp (°C)	Small buds without mitochondria (% of small-budded cells)
Wild type	25	11.5
*ypt11*Δ	25	26.7
ypt11^{V246D}	25	12.4
Wild type	37	10.6
*ypt11*Δ	37	29.2
ypt11^{V246D}	37	24.5
Wild type (diploid)	25	15.2
*ypt11*Δ/*ypt11*Δ (diploid)	25	34.2

[a] Over 200 cells with a small bud (whose bud diameter is approximately 1.1- to 1.5-fold of the diameter of the bud neck) were observed. Cells were cultured at 25°C, and cells at early log phase were harvested for observation (25°C) or shifted to 37°C and harvested 50 min after the shift (37°C). The cells were stained with DASPMI for visualization of mitochondria.

tent to that of wild-type cells at 25°C, and only 12% of the small-budded cells failed to transmit mitochondria to the bud. However, 50 min after the shift to 37°C, about 25% of the small buds of *ypt11*^{V246D} cells did not possess detectable mitochondria whereas the temperature shift did not affect the mitochondrial transmission to the bud of wild-type cells (Table 1). Therefore, these results strongly suggest that Ypt11p acts directly and positively on efficient transmission of mitochondria toward the bud.

Mutational analysis of *YPT11*. To investigate the site of binding of Ypt11p to Myo2p, we introduced mutations into *YPT11* and investigated the interaction between the mutant Ypt11p and Myo2p. We examined mutations corresponding to dominant inhibitory mutations in other small GTPase genes and disrupting the effector domain of Ypt11p (2). However, compared with the wild-type *YPT11*, Western blot analysis revealed that *YPT11* expression was reduced in most mutants, except for *ypt11*^{1144N}, whose product carried a substitution of Asn for Ile 144 in the Ypt11p effector domain, and *ypt11*^{G40D}, whose product carried a substitution of Asp for the Gly 40 in the first GTP-binding and hydrolysis motif. Expression of *ypt11*^{1144N} and *ypt11*^{G40D} from the constructs for the USA_{GAL}-binding domain fusion of Ypt11p was almost equal to that of wild-type *YPT11* (Fig. 5A, bottom). Therefore, we characterized these mutant *ypt11*s further. The mutation, corresponding to *ypt11*^{1144N}, in the rab-type small GTPases disrupts their effector domain and the interaction with their effectors (20). The substitution of Asp for the conserved Gly, proximal to Lys in the GXXXXGK(T/S) motif, freezes the Ras2p GTPase in the GDP-binding inactive form (27), and the substitution corresponds to *ypt11*^{G40D}.

Neither Ypt11p^{1144N} nor Ypt11p^{G40D} displayed a two-hybrid interaction with Myo2p (Fig. 5A), indicating that the effector domain and the first motif for GTP binding and hydrolysis of Ypt11p are critical for the interaction with Myo2p. In the coimmunoprecipitation assay, a reduced amount of Myo2p was coprecipitated with Ypt11p^{G40D}, compared with the amount precipitated with wild-type Ypt11p, and no detectable amount of Myo2p was coprecipitated with Ypt11p^{1144N} (Fig. 1B). Therefore, these results indicate that the complex formation between Myo2p and Ypt11p requires the effector domain of Ypt11p and the intact GTP hydrolysis domain. These observations suggest that Myo2p is an effector of Ypt11p.

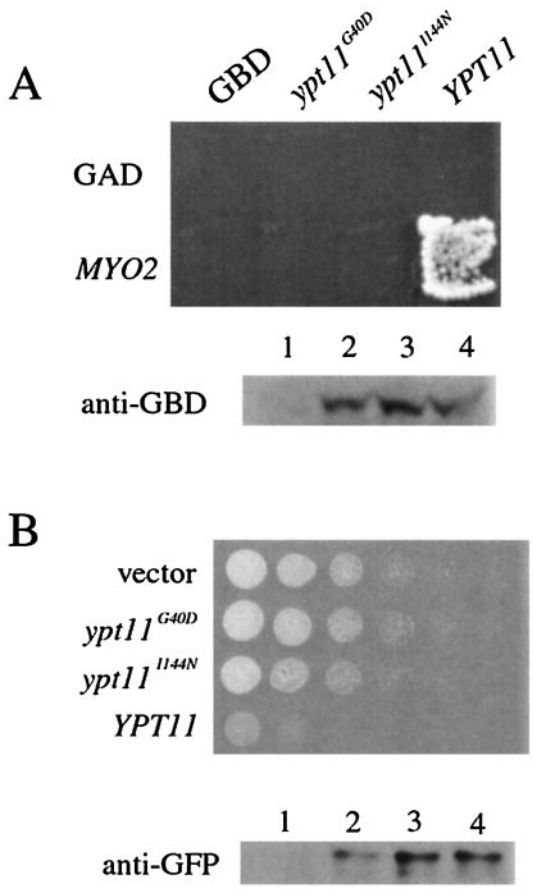

FIG. 5. Characterization of *ypt11*^{G40D} and *ypt11*^{1144N}. (A) Two-hybrid interaction of mutant Ypt11p with Myo2p. (Top) Reporter cells (strain PJ69-4A) carrying *HIS3* and *ADE2* under the control of USA_{GAL} were transformed with pGBDU-C1-based constructs for USA_{GAL}-binding domain fusion of the indicated *YPT11* or pGBDU-C1 for a control (GBD) and with pGAD-C1-based constructs for *trans*-activator domain fusion of *MYO2* or pGAD-C1 for a control (GAD). Cells were streaked on SC medium lacking uracil, leucine, histidine, and adenine, where two-hybrid interactions were detected as cell growth. (Bottom) Relative amounts of the USA_{GAL}-binding domain (GBD) fusion of Ypt11p in the cells above (lane 1, control; lane 2, *ypt11*^{G40D}; lane 3, *ypt11*^{1144N}; lane 4, *YPT11*) were analyzed by Western analysis using anti-GBD antibodies, showing that the mutations in *YPT11* did not affect the *YPT11* expression from the constructs. (B) Effect of overexpression of mutant *YPT11* on cells growth. (Top) *ypt11*Δ cells (strain yTO001) with a control plasmid (vector) or with plasmids for overexpression of indicated *YPT11* under the control of the *GAL1* promoter were spotted on SCGal plates lacking uracil and incubated at 30°C for 3 days. The cell suspension for the spot was diluted 10-fold from left to right. (Bottom) *ypt11*Δ cells (strain yTO001) with a control plasmid (lane 1) or with plasmids for overexpression of *YPT11*^{G40D} (lane 2), *YPT11*^{1144N} (lane 3), or wild-type *YPT11* (lane 4) were cultured in SCGal medium lacking uracil for 2 h and harvested. The same amount of proteins in each cell lysate was analyzed by Western blotting using anti-GFP antibodies.

Overexpression of either *ypt11*^{1144N} or *ypt11*^{G40D} under the control of the *GAL1* promoter did not inhibit cell growth (Fig. 5B, top) and did not cause accumulation of mitochondria in the bud (Table 2), whereas that of wild-type *YPT11* did. Since

TABLE 2. Mitochondrial distribution in cells with a middle-sized bud, overexpressing mutant *ypt11*[a]

Plasmid	% of cells with:	
	Normal mitochondria	Mitochondria accumulated in the bud
Vector	100	<0.5
YPT11	18	82
ypt11^{G40D}	100	<0.5
ypt11^{1144N}	100	<0.5

[a] *ypt11*Δ cells (strain yTO001) with a control plasmid (vector) or with plasmids for overexpression of the indicated *YPT11* (wild-type *YPT11, ypt11*^{G40D}, or *ypt11*^{1144N}) under the control of the *GAL1* promoter were cultured until early log phase in SCraffinose lacking uracil, shifted into SCGal medium lacking uracil for induction, incubated for 4 h at 25°C, stained with DASPMI, and observed to count the numbers of budded cells with a normal distribution of mitochondria or with mitochondria accumulated in the bud. More than 200 cells with a middle-sized bud were observed.

the expression of *ypt11*^{1144N} by the *GAL1* promoter was almost equal to that of wild-type *YPT11* (Fig. 5B, bottom), these results strongly suggest that Ypt11p requires coupling with its effector(s) at the effector domain to inhibit cell growth and to accumulate mitochondria in the bud.

Phenotypes of *myo2-338* cells. The *ypt11*^{1144N} and *ypt11*^{G40D} mutations possibly disrupt the interaction with all the effectors of Ypt11p. Therefore, although it is suggested that Myo2p is a putative effector of Ypt11p, it is unclear whether Myo2p is the effector which is responsible for the effect of Ypt11p on cell growth and mitochondrial distribution. To examine whether Myo2p is this effector, we performed a reciprocal analysis by isolating *myo2* mutants. We mutagenized a limited *MYO2* region that encompassed the C-terminal tail domain (amino acid residues 827 to 1569) using PCR mutagenesis (6) and isolated 28 *myo2* mutants that showed temperature-sensitive growth phenotypes (Ts$^-$). Of these, the *myo2-338* mutation was isolated as the mutation that nullified the inhibitory effect of overexpressed *YPT11* on cell growth. *myo2-338* cells overexpressing *YPT11* grew well (Fig. 6A, sector b in the galactose-containing medium), whereas wild-type cells overexpressing *YPT11* did not (sector c in the galactose-containing medium). Moreover, in *myo2-338* cells, the *YPT11* activity required to accumulate mitochondria in the bud was reduced drastically. During *YPT11* overexpression, more than 80% of wild-type cells with a middle-sized bud accumulated mitochondria in the bud whereas about 95% of *myo2-338* cells with a middle-sized bud displayed normal mitochondrial distribution (Fig. 6B). Two-hybrid analysis showed that Myo2-338p failed to interact with Ypt11p (Fig. 6C), indicating that the *myo2-338* mutation weakens this interaction. Therefore, along with the results from the *YPT11* mutations, we conclude that Myo2p acts as the effector of Ypt11p for the Ypt11p effect on cell growth and mitochondrial distribution.

The morphology of mitochondria in *myo2-338* cells was normal at both the permissive and nonpermissive temperatures (Fig. 6E). This observation is consistent with the finding that disruption of *YPT11* did not cause any defect in mitochondrial morphology (data not shown).

Phenotypes of *myo2-573* cells. Although it has not been reported previously that Myo2p participates in mitochondrial distribution, our findings suggest that Myo2p plays a role, at least, by acting as the Ypt11p effector. Moreover, characterization of *myo2-573* cells revealed that Myo2p plays an essential role in mitochondrial distribution. The *myo2-573* mutation was isolated as the mutation showing a synthetic lethal interaction with *ypt11*Δ (Fig. 7) from the *myo2* Ts$^-$ mutants described above. Even at a permissive temperature (25°C), about 70% of *myo2-573* large-budded cells accumulated mitochondria at the bottom of the mother cells and exhibited the defect in mitochondrial transmission toward the bud, whereas all of the wild-type large-budded cells showed normal distribution of mitochondria (i.e., extending from the bottom of the mother cells to the bud tip [Fig. 8A, top left]). At 1 h after transfer to the nonpermissive temperature (37°C), about 89% of *myo2-573* large-budded cells exhibited the defect. Unlike other *myo2* mutant cells, e.g., *myo2-66* cells (17), *myo2-573* cells did not become enlarged, unbudded, and depolarized. Other than a slight increase of the unbudded population in culture, the morphology of *myo2-573* cells was similar to that of wild-type cells, even at a nonpermissive temperature (Fig. 8A). We observed the polarized organization of actin filaments (i.e., cortical patches of actin filaments localizing in the bud exclusively and actin cables running through the mother cell [Fig. 8A]). We observed normal vacuole inheritance at both permissive and nonpermissive temperatures in *myo2-573* cells (Fig. 8B). After an 8-h incubation at 37°C, we did not observe any *myo2-573* cells carrying two nuclei in the cell, a consequence of the defect in spindle orientation. Therefore, these observations suggest that the *myo2-573* defect affects mitochondrial distribution specifically.

To confirm this, we carried out quantitative analysis of actin organization, Kar9p localization for spindle orientation, and localization of secretory vesicles, all of which involve Myo2, in *Myo2-573* cells. At 25°C, whereas about 70% of *myo2-573* large-budded cells displayed the defect in mitochondrial distribution, nearly 100% of the cells possessed a polarized organization of actin cytoskeleton, as in wild-type cells. For proper orientation of the spindle, Myo2p localizes Kar9p at the bud tip (44). In about 61% of the large-budded *myo2-573* cells, GFP-tagged Kar9p was localized at the bud tip (in wild-type cells, about 68% of the large-budded cells did so). We observed localization of secretory vesicles by using GFP-tagged Sec2p, since Sec2p is associated with secretory vesicles (11). GFP-tagged Sec2p was detected at the bud tip of small-budded cells, showing a polarized distribution of secretory vesicles (Fig. 8C). About 83% of small-budded *myo2-573* cells localized Sec2p at the bud tip, and about 89% of small-budded wild-type cells did so. The *myo2-573* defect in mitochondrial distribution was enhanced at 37°C; after a 0.5- and 1-h incubation at 37°C, 83 and 89% of *myo2-573* large-budded cells, respectively, showed the mitochondrial defect, whereas all of the wild-type large-budded cells distributed mitochondria properly at 37°C. In contrast to the mitochondrial defect, at 2 h after the shift to 37°C, about 98% of *myo2-573* cells showed a polarized organization of the actin cytoskeleton (100% of wild-type cells did so) and about 43% of small-budded *myo2-573* cells localized Sec2p at the bud tip (about 71% of the small-budded wild-type cells did so). Considering that the polarized localization of Sec2p is completely disrupted in *myo2-66* cells (11), the fact that about 44% of the *myo2-573* small-budded cells still retained polarized localization of Sec2p under the restrictive

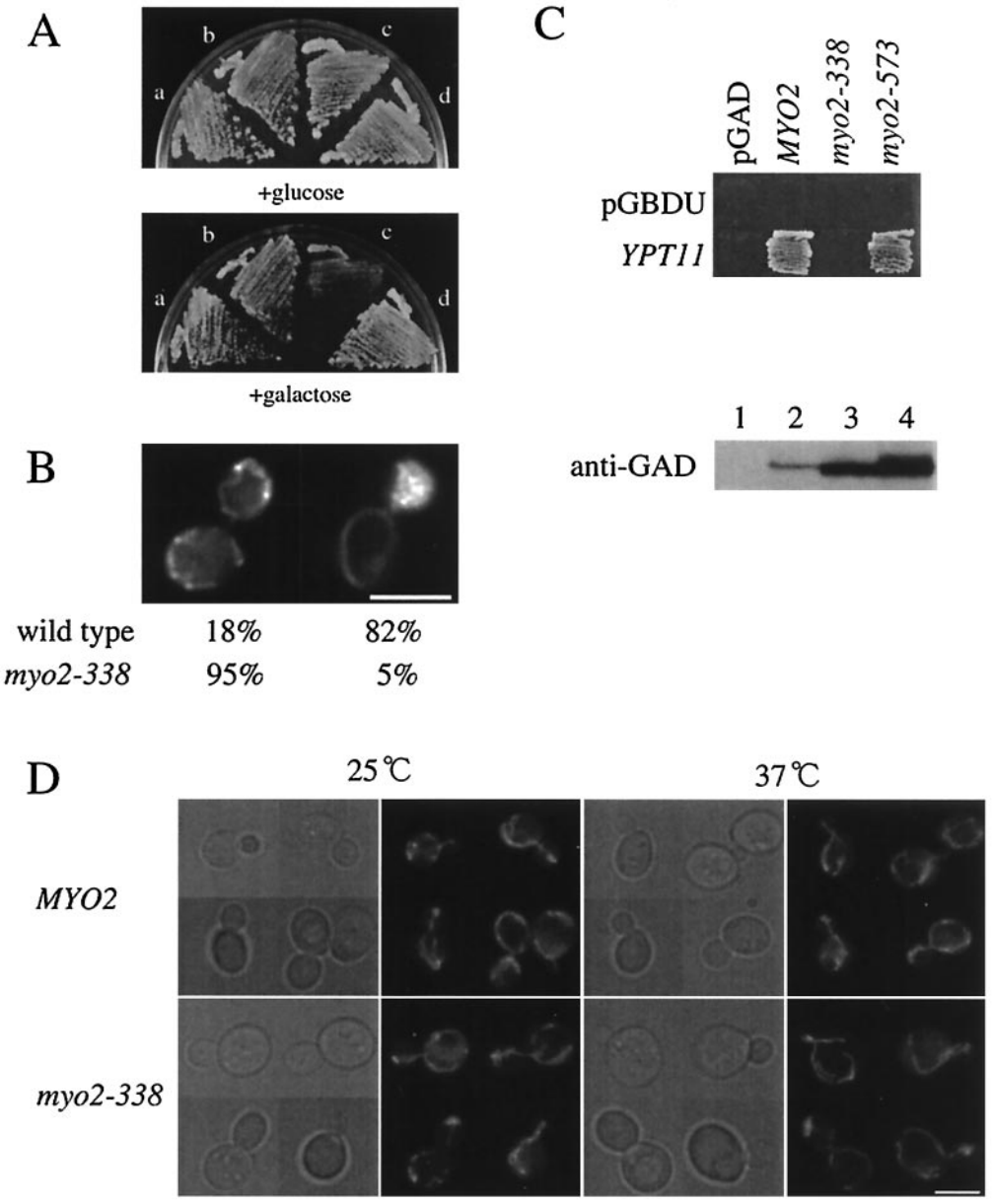

FIG. 6. Phenotypes of *myo2-338* cells. (A) Effect of overexpression of *YPT11* on *myo2-338* cells. *myo2-338* cells (strain yTO014 [a and b]) and wild-type cells (strain YPH499 [c and d]) with YIpUGAL7-YPT11 (b and c), *YPT11* under the control of the *GAL7* promoter, or without YIpUGAL7-YPT11 (a and d) were streaked on YPD (+glucose) and YPG (+galactose) plates and incubated at 30°C for 3 days. (B) Mitochondrial distribution in *myo2-338* cells overexpressing *YPT11*. Wild-type cells (strain YPH499) and *myo2-338* cells (strain yTO014) with YIpGAL7-YPT11 were cultured until early log phase in SC raffinose, shifted into SCGal medium for induction, incubated for 4 h at 25°C, stained with DASPMI, and observed to count the number of cells with a normal distribution of mitochondria (left) or with mitochondria accumulated in the bud (right). More than 200 of cells with a middle-sized bud were observed. (C) Two-hybrid interaction of mutant Myo2p with Ypt11p. (Top) Reporter cells (strain PJ69-4A) were transformed with pGBDU-C1 (pGBDU) for a control or pK027, a pGBDU-C1-based plasmid for Ypt11p fused with the UAS_{GAL}-binding domain (*YPT11*), and pGAD-C1-based constructs of *MYO2* (pK016 for *MYO2,* pK017 for *myo2-338,* pK018 for *myo2-573*) or pGAD-C1 for a control (pGAD). The cells were streaked on SC medium lacking uracil, leucine, histidine, and adenine, where two-hybrid interactions were detected as cell growth. (Bottom) Relative amounts of the fusion proteins of Myo2p with the *trans*-activator domain (GAD) in the cells above were analyzed by Western blotting using anti-GAD antibodies (lane 1, control; lane 2, cells with pK016, lane 3, cells with pK017, lane 4, cells with pK018). *myo2-338* from the pGAD-based construct was expressed more strongly than *MYO2* from the pGAD-based construct; however, two-hybrid interaction was not detected. (D) Morphology of mitochondria in *myo2-338* cells. Wild-type cells (strain YPH499, *MYO2*) and *myo2-338* cells (strain yTO014, *myo2-338*), producing mitochondrion-targeting GFP, were cultured until early log phase at 25°C (25°C), shifted to 37°C, and incubated for 2 h (37°C). Phase-contrast images (left) and GFP signals (right) of each culture are shown. Bars, 5 μm.

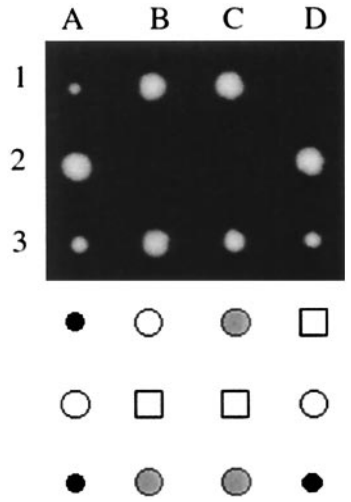

FIG. 7. Synthetic growth defect of *myo2-573* with *ypt11*Δ. *myo2-573*/+ *ypt11*Δ/+ heterozygous diploid cells were sporulated, and three sets of tetrads (1 to 3), dissected, are shown in the upper panel. The genotypes of the spore clones are indicated in the lower panel: wild-type spores (open circles), *ypt11*Δ spores (gray circles), *myo2-573* spores (black circles), and *myo2-573 ypt11*Δ spores (squares). The *myo2-573* spore clones did not form visible colonies after incubation for 3 days at 25°C in combination with *ypt11*Δ, whereas *ypt11*Δ *MYO2* spore clones and *myo2-573 YPT11* spore clones did so. After prolonged incubation, several *myo2-573 ypt11*Δ spore clones formed microcolonies, which were difficult to repropagate.

conditions suggests that the *myo2-573* defect is not critical for the localization of secretory vesicles. From the above observation, we conclude that the *myo2-573* defect affects mitochondrial distribution specifically.

In both higher eukaryotes and yeast, mitochondria are partly colocalized with and connected to the peripheral endoplasmic reticulum (ER). Defects in the peripheral ER in yeast lead to mitochondrial abnormality (29). Although the morphology of the ER is independent of the actin cytoskeleton, we examined whether the *myo2-573* defect causes abnormality in the ER structure. Using GFP-tagged Sec63p (an ER protein), we observed normal morphology of the peripheral ER in *myo2-573* cells, extending near the cell cortex of both mother cells and buds and forming a network morphology (data not shown). Therefore, it is unlikely that the defect in mitochondrial distribution in *myo2-573* cells is induced by the defect in the ER morphology.

We examined the cellular localization of Myo2-573p using the GFP-tag. In cells carrying a GFP-tagged version of *myo2-573*, replacing the wild-type *MYO2* allele, Myo2-573p localized at the bud site of the emerging bud, at the bud cortex of the growing bud, and at the bud neck in M phase (Fig. 8D right). The cellular localization is almost identical to that of Myo2p (Fig. 8D left). These results are consistent with the finding that the *myo2-573* defect does not affect Myo2p function other than for mitochondrial distribution.

We analyzed the interaction between Myo2-573p and Ypt11p by a two-hybrid assay. We detected the two-hybrid interaction between Myo2-573p and Ypt11p (Fig. 6C), suggesting that Myo2-573p can interact with Ypt11p. A high dose of *YPT11* suppressed the temperature-sensitive growth defect of *myo2-573* cells; however, it did not suppress that of *myo2-338* cells (Fig. 8E). These results strongly suggest that Myo2-573p can interact with Ypt11p physically and functionally whereas Myo2-338p has lost both these interactions.

Ypt11p localization in cells carrying mutations that affect the Myo2p-Ypt11p interaction. GFP-tagged Ypt11p was concentrated in growing buds (Fig. 9), as observed using HA-tagged Ypt11p (Fig. 2). However, in *myo2-338* cells, the exclusive localization of Ypt11p to the bud was lost. Instead, Ypt11p was dispersed and observed around the nuclei and cell cortex of both mother cells and the bud, suggesting that a part of Ypt11p localized to the ER (Fig. 9). GFP-tagged Ypt11p^{G40D} and Ypt11p^{1144N} did not localize exclusively in the bud; instead, they showed similar localization to that of Ypt11p in *myo2-338* cells (data not shown). These results suggest that Ypt11p requires interaction with Myo2p for the bud localization. Ypt11p accumulated in the buds of *myo2-573* cells (Fig. 9), consistent with the result that the *myo2-573* mutation did not reduce the two-hybrid interaction between Myo2p and Ypt11p (Fig. 6C).

DISCUSSION

The interactions between a rab-type small GTPase and a class V myosin in mammals have been reported (9). In the budding yeast, we found an interaction between Myo2p and Ypt11p. These facts suggest that the complex formation between a rab-type small GTPase and a class V myosin is evolutionarily conserved from yeast to mammals and is important for living cells. Two-hybrid analysis of the interaction between myosin-Vb and Rab11a shows that myosin-Vb interacts with Rab11a in the GTP-bound form via the effector domain of Rab11a (20). Like the interaction in mammalian cells, the interaction between Ypt11p and Myo2p is abolished by the *ypt11^{1144N}* mutation in the effector domain and reduced by the *ypt11^{G40D}* mutation, presumably freezing the GTPase in the GDP-bound form (Fig. 5A). Small GTPases interact with their effector through the effector domain when in the GTP-bound active form. Therefore, the mutational study of Ypt11p suggests that Myo2p is a putative effector of Ypt11p. Since both mutations, *ypt11^{1144N}* and *ypt11^{G40D}*, nullified the Ypt11p effect on mitochondrial distribution and cell growth (Table 2; Fig. 5B), these effects of Ypt11p are exerted by its effector(s). Using yeast genetics, we successfully isolated a new *myo2* allele (*myo2-338*) that cancels these Ypt11p effects (Fig. 6A and B). The *myo2-338* mutation abolished the two-hybrid interaction with Ypt11p (Fig. 6C). These results strongly suggest that Myo2p acts as the effector of Ypt11p for these effects and that their complex formation is critical for these Ypt11p functions. Overexpression of *YPT11* resulted in the accumulation of mitochondrial in the bud, and dysfunction of *YPT11* induced a partial delay of the mitochondrial transmission toward the bud (Fig. 3B and 4; Table 1). These results strongly suggest that Ypt11p plays a positive and direct role in mitochondrial transmission toward the bud. In addition, we revealed that Myo2p plays a crucial role in the polarized distribution of mitochondria by the characterization of the novel *myo2* allele (*myo2-573*), causing the defect specifically in mitochondrial distribution (Fig. 8). Taken together, these results show that Myo2p is the effector of Ypt11p for accumulating mitochondria in the

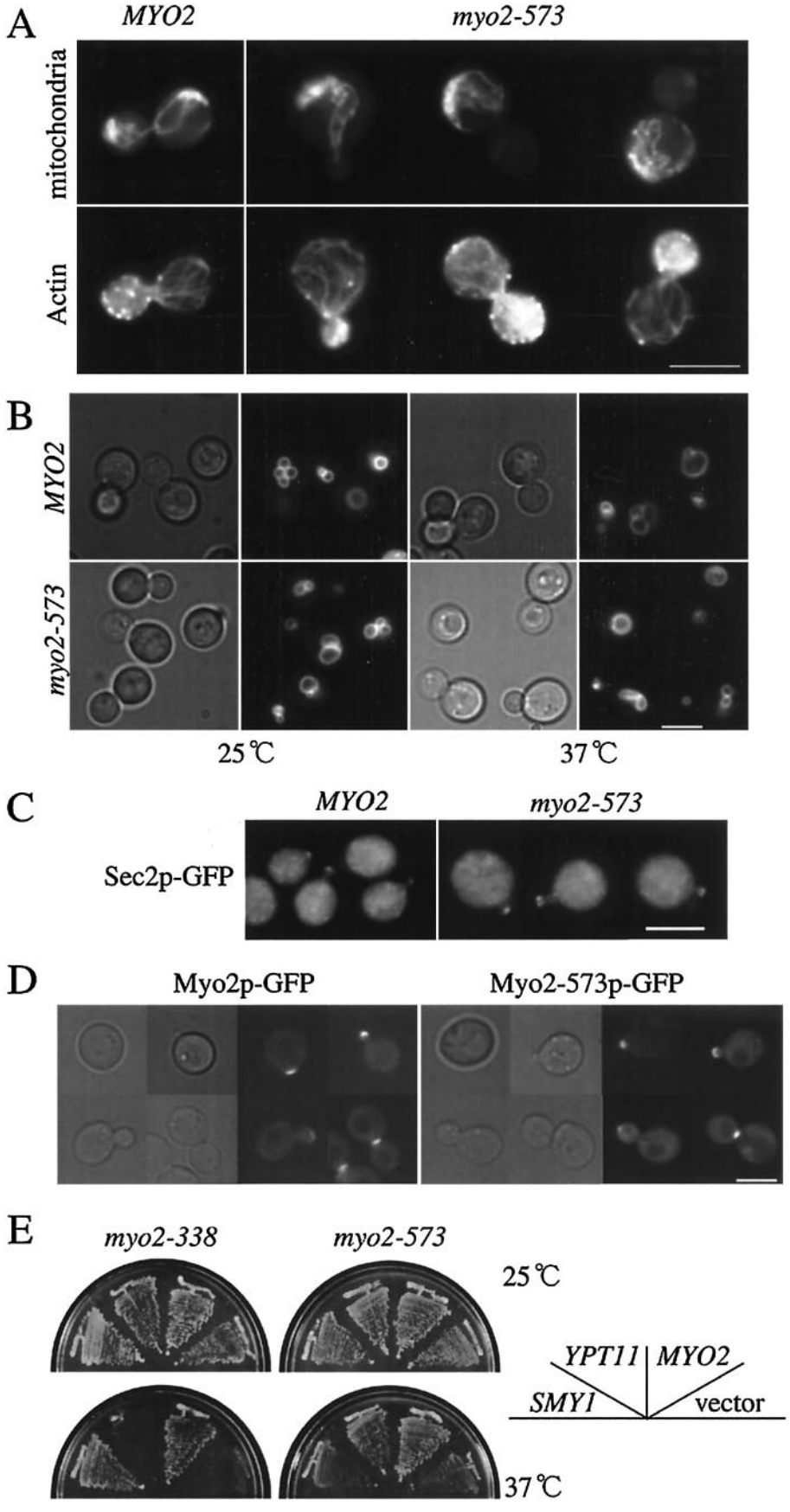
A
MYO2
myo2-573
mitochondria
Actin
B
MYO2
myo2-573
25℃
37℃
C
MYO2
myo2-573
Sec2p-GFP
D
Myo2p-GFP
Myo2-573p-GFP
E
myo2-338
myo2-573
25℃
YPT11
MYO2
SMY1
vector
37℃

bud and that the role of the complex formation between Ypt11p and Myo2p is to facilitate the Myo2p function for mitochondrial distribution.

Mitochondria are essential organelles in eukaryotes and are inherited by daughter cells from mother cells. Actin is essential for mitochondrial distribution in the budding yeast. The loss of actin function abolishes mitochondrial motility and results in abnormal mitochondrial morphology (10, 22), indicating that actin plays essential roles in producing mitochondrial motility and retaining their network morphology. Although the role of actin in mitochondrial distribution is established, the role of myosins has been unclear. Moreover, it has been reported that myosins do not participate in mitochondrial motility, because the mutations in any myosins in yeast, including *myo2-66*, do not affect the velocity of mitochondrial movement (35). Defects in the distribution and morphology of mitochondria were previously reported in *myo2-66* cells (35). However, the changes correlate with severe defects in the polarized organization of the actin cytoskeleton and therefore are thought to be induced by the depolarized actin cytoskeleton. We isolated *myo2-573* mutant cells, in which Ypt11p, a positive regulator for mitochondrial distribution, is essential (Fig. 7). In *myo2-573* cells, mitochondrial distribution was defective whereas the actin cytoskeleton was properly organized and organelles other than mitochondria were distributed normally (Fig. 8). Therefore, the *myo2-573* defect in mitochondrial distribution is the first evidence that myosin plays a crucial role in mitochondrial distribution. Myo2-573p underwent a two-hybrid interaction with Ypt11p (Fig. 6C), and the *myo2-573* defect was suppressed by a high dose of *YPT11* (Fig. 8E), suggesting strongly that Myo2-573p retains affinity for Ypt11p. The *myo2-573* mutation induces six substitutions (Val 1189 to Ala, Val 1288 to Gly, Lys 1500 to Met, Pro 1529 to Ser, Glu 1546 to Gly, and Lys 1559 to Arg), and none of these overlap with any critical residues, whose substitution is reported to induce defects in the transport of secretory vesicles or vacuoles (8, 32). It is conceivable that the *myo2-573* mutation reduces the affinity of Myo2p for a factor for mitochondrial distribution.

For proper distribution of mitochondria, polarization of the mitochondrial movement is essential because mitochondrial distribution is defective in *tpm1*Δ cells, where mitochondria move at wild-type velocity but not in a polarized fashion (35). In *tpm1*Δ cells, actin cables are selectively lost, suggesting that polarization of mitochondrial movement requires actin cables.

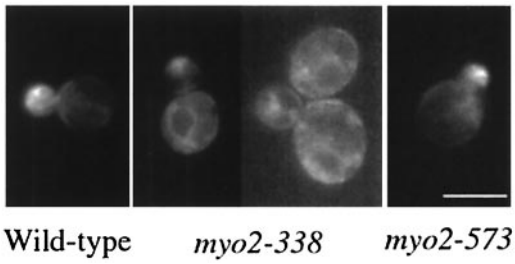

FIG. 9. Cellular localization of Ypt11p in mutant *myo2* cells. A high-copy-number plasmid for production of Ypt11p tagged with GFP at its N terminus (GFP-Ypt11p) under the control of the *YPT11* promoter (pK022) was introduced into the indicated cells (wild-type, strain YPH499; *myo2-338*, strain yTO014; *myo2-573,* strain yTO015). The cells were cultured at 25°C, harvested at early log phase, and observed. Bar, 5 μm.

Mitochondria partly colocalize with the actin structure (10, 34, 35), and in *myo2-573* cells, connections between mitochondria and the actin structure are disrupted in the bud (Fig. 8A). Therefore, it is possible that Myo2p may polarize mitochondrial movement by forming a connection between the actin structure and mitochondria. Using cell fractionation analysis, we examined whether Myo2p interacts with mitochondria directly, but we obtained no evidence. Although this may suggest that the connection between Myo2p and mitochondria is transient, we cannot exclude the possibility that the involvement of Myo2p in mitochondrial distribution is indirect, such that Myo2p transports the mitochondrion-tethering factor along the actin cytoskeleton and the transported factor establishes a polarized distribution of mitochondria. In either case, it is plausible that Ypt11p accelerates the interaction of Myo2p with mitochondria or the mitochondrion-tethering factor by complex formation with Myo2p. In *YPT11*-overexpressing cells, Myo2p was highly concentrated in the bud where mitochondria had accumulated (Fig. 3E). This observation is consistent with the idea that Ypt11p enhances the affinity of Myo2p for mitochondria. In addition, this ability of Ypt11p to concentrate Myo2p in the bud may also explain why Ypt11p is identified as a high-dose suppressor of the *myo2-66* defect; that is, the increase of Myo2p in the bud compensates for the decreased Myo2p activity by the *myo2-66* mutation and restores the essential Myo2p activity for bud formation.

FIG. 8. Phenotypes of *myo2-573* cells. (A) Actin cytoskeleton and mitochondrial distribution in *myo2-573* cells. Wild-type cells (strain YPH499, *MYO2*) and *myo2-573* cells (strain yTO015, *myo2-573*) producing mitochondrion-targeting GFP were cultured until early log phase at 25°C, fixed, and stained with rhodamine-phalloidin to visualize actin. GFP of mitochondria (bottom) and actin staining of the same cells (top) are shown. (B) Distribution of vacuoles in *myo2-573* cells. Wild-type cells (strain YPH499, *MYO2*) and *myo2-573* cells (strain yTO015, *myo2-573*) were cultured until early log phase at 25°C (25°C), shifted to 37°C, and incubated for 2 h (37°C). The cells were stained with FM4-64. Phase-contrast images (left) and vacuole staining (right) of each culture were shown. (C) Localization of Sec2p. Wild-type cells (strain YPH499, *MYO2*) and *myo2-573* cells (strain yTO015, *myo2-573*), producing GFP-tagged Sec2p, were cultured until early log phase at 25°C, shifted to 37°C, and incubated for 2 h. GFP signals were detected at the tips of the small-budded cells. (D) Localization of Myo2-573p. The *myo2-573* locus of the *myo2-573* cells (strain yTO015 with the disruption of the *TRP1* marker with *HIS3*) was replaced with *myo2-573* fused to GFP for producing Myo2-573p tagged at the C terminus with GFP under the control of its own promoter (Myo2-573p-GFP [right]). The *MYO2* locus of wild-type cells (strain YPH499) was replaced with the GFP-tagged version of *MYO2* (Myo2-GFP [left]). GFP signals (right) and phase-contrast images (left) are shown. Bars, 5 μm. (E) Suppression of the *myo2* defects by a high-dose suppressor of *myo2-66*. *myo2-338* cells (strain yTO014, *myo2-338*) and *myo2-573* cells (strain yTO015, *myo2-573*), with an indicated plasmid (vector, pYO326 for a control, *MYO2*; YCp50MYO2, a low-copy-number plasmid carrying *MYO2; YPT11,* pK008, a high-copy-number plasmid carrying *YPT11;* SMY1, pSMY1, a high-copy-number plasmid carrying SMY1) were streaked on an SC plate lacking uracil and incubated for 3 days at the indicated temperatures.

It is suggested that in mammalian cells, Rab11a and Rab27a target the myosin-V motor to the membranes where the rab-type small GTPases localize. We have no evidence that Ypt11p localizes to mitochondria. However, in the absence of the interaction with Myo2p, Ypt11p accumulated on the ER membrane (Fig. 9, middle). The peripheral ER extends near the cell cortex of both the mother cell and the bud and forms an actin-independent network morphology. In addition to actin cables, mitochondria are partly colocalized with and connected to the peripheral ER (29). Therefore, it is possible that Ypt11p localizes at the ER subdomain, interacting with mitochondria, and recruits Myo2p to the subdomain to affect the polarized distribution of mitochondria.

Although Ypt11p possibly plays a positive and direct role in mitochondrial transmission toward the bud, loss of *YPT11* did not disrupt morphology and distribution of mitochondria, except for the partial delay at the stage of small-budded cells. In addition, the extent of the delay of mitochondrial transmission in *ypt11*Δ cells varied with the cellular conditions. The delay was enhanced in diploid cells (Table 1), but we did not observe any delay of the transmission in the bud of the *ypt11*Δ cells, released from the arrest by α-factor (data not shown). These results may suggest that Ypt11p-dependent facilitation of the Myo2p activity on mitochondrial transmission is crucial under restricted cellular conditions. Alternatively, we cannot exclude the possibility that yeast cells possess another factor that is functionally redundant with Ypt11p. Smy1p is similar to Ypt11p in some features; that is, Smy1p acts as a high-dose suppressor of the *myo2-66* defect and shows two-hybrid interaction with the C-terminal tail domain of Myo2p (3). However, *smyl*Δ *ypt11*Δ cells grew normally (data not shown), suggesting that Ypt11p and Smy1p do not share an essential function. In addition, the roles of Ypt11p is different from that of Smy1p in *myo2-573* cells; namely, these cells require Ypt11p but not Smy1p for growth (i.e., *myo2-573* is synthetic lethal with *ypt11*Δ, but *myo2-573 smy1*Δ cells grow as well as *myo2-573* cells), and a high dose of *YPT11* rescued the *myo2-573* defect but a high dose of *SMY1* did not (Fig. 8E). Therefore, it is unlikely that Smy1p is functionally redundant with Ypt11p.

Since the distribution of cellular organelles, except for mitochondria, was not affected by *YPT11* overexpression (see Fig. 3C for actin and vacuole), the function of Ypt11p seems to be relatively specialized for mitochondrial distribution. However, *YPT11*-overexpressing cells cease to grow, independent of the mitochondrial content of cells, and become unbudded, suggesting that Ypt11p may have a function in bud emergence apart from its function for mitochondrial distribution. This Ypt11p function also requires complex formation with Myo2p, since the Ypt11p activity in inhibiting bud emergence is abolished by mutations such as *myo2-338*, *ypt11*^{1144N}, and *ypt11*^{G40D}, which disrupt the Myo2p-Ypt11p interaction.

The *myo2-338* mutation, which abolished the interaction with Ypt11p, induces three substitutions (Leu 1474 to Ser, Glu 1484 to Gly, and Asp 1511 to Gly) of the residues, which are conserved among class V myosins, near the C terminus. For example, Leu 1474, Glu 1484, and Asp 1511 of Myo2p correspond to Ile 512, Glu 526, and Asp 553 of rabbit myosin-Vb, respectively. Interestingly, the myosin-Vb region, containing these residues (amino acids 512 to 553) overlaps with the region from amino acids 538 to 553, which is critical for the two-hybrid interaction with Rab11a (20). These observations may suggest that these conserved residues constitute the binding domain with rab-type small GTPases.

Although actin is essential for mitochondrial distribution in the budding yeast, microtubules and microtubule-dependent motor proteins play critical roles in mitochondrial transport in higher eukaryotes and microfilaments play a less clear role (43). However, in several cases, microfilament-dependent mitochondrial movement has been reported, such as in the neuronal axons of mammals (28) and in the photoreceptor cells (36) and Malpighian tubule cells (4) of insects. Our finding of the involvement of myosin in the polarized distribution of mitochondria may provide a clue to clarify the role of microfilaments in mitochondrial distribution in higher eukaryotes.

ACKNOWLEDGMENTS

We thank E. Craig for providing the two-hybrid screening system, S. Nishikawa and T. Endo for providing the plasmid for the GFP fused Cox4 signal sequence, T. Rapoport for providing the plasmids for the GFP fused Sec63p, S. Yosihda and R. Matsui for helpful discussion, and S. Naramoto for technical assistance.

The work was supported by a grant from Monbu-Kagaku-Sho.

REFERENCES

1. **Bahadoran, P., E. Aberdam, F. Mantoux, R. Busca, K. Bille, N. Yalman, G. de Saint-Basile, R. Casaroli-Marano, J. P. Ortonne, and R. Ballotti.** 2001. Rab27a: a key to melanosome transport in human melanocytes. J. Cell Biol. **152:**843–850.
2. **Barbacid, M.** 1987. *ras* genes. Annu. Rev. Biochem. **56:**779–827.
3. **Beningo, K. A., S. H. Lillie, and S. S. Brown.** 2000. The yeast kinesin-related protein Smy1p exerts its effects on the class V myosin Myo2p via a physical interaction. Mol. Biol. Cell **11:**691–702.
4. **Bradley, T. J., and P. Satir.** 1979. Evidence of microfilament-associated mitochondrial movement. J. Supramol. Struct. **12:**165–175.
5. **Brown, S. S.** 1999. Cooperation between microtubule- and actin-based motor proteins. Annu. Rev. Cell Dev. Biol. **15:**63–80.
6. **Cadwell, R. C., and G. F. Joyce.** 1992. Randomization of genes by PCR mutagenesis. PCR Methods Appl. **2:**28–33.
7. **Carlson, M., and D. Botstein.** 1982. Two differentially regulated mRNAs with different 5′ ends encode secreted with intracellular forms of yeast invertase. Cell **28:**145–154.
8. **Catlett, N. L., J. E. Duex, F. Tang, and L. S. Weisman.** 2000. Two distinct regions in a yeast myosin-V tail domain are required for the movement of different cargoes. J. Cell Biol. **150:**513–526.
9. **Deacon, S. W., and V. I. Gelfand.** 2001. Of yeast, mice, and men. Rab proteins and organelle transport. J. Cell Biol. **152:**F21–F24.
10. **Drubin, D. G., H. D. Jones, and K. F. Wertman.** 1993. Actin structure and function: roles in mitochondrial organization and morphogenesis in budding yeast and identification of the phalloidin-binding site. Mol. Biol. Cell **4:**1277–1294.
11. **Elkind, N. B., C. Walch-Solimena, and P. J. Novick.** 2000. The role of the COOH terminus of Sec2p in the transport of post-Golgi vesicles. J. Cell Biol. **149:**95–110.
12. **Gietz, R. D., and A. Sugino.** 1988. New yeast-*Escherichia coli* shuttle vectors constructed with in vitro mutagenized yeast genes lacking six-base pair restriction sites. Gene **74:**527–534.
13. **Hill, K. L., N. L. Catlett, and L. S. Weisman.** 1996. Actin and myosin function in directed vacuole movement during cell division in *Saccharomyces cerevisiae.* J. Cell Biol. **135:**1535–1549.
14. **Hume, A. N., L. M. Collinson, A. Rapak, A. Q. Gomes, C. R. Hopkins, and M. C. Seabra.** 2001. Rab27a regulates the peripheral distribution of melanosomes in melanocytes. J. Cell Biol. **152:**795–808.
15. **James, P., J. Halladay, and E. A. Craig.** 1996. Genomic libraries and a host strain designed for highly efficient two-hybrid selection in yeast. Genetics **144:**1425–1436.
16. **Jedd, G., C. Richardson, R. Litt, and N. Segev.** 1995. The Ypt1 GTPase is essential for the first two steps of the yeast secretory pathway. J. Cell Biol. **131:**583–590.
17. **Johnston, G. C., J. A. Prendergast, and R. A. Singer.** 1991. The *Saccharomyces cerevisiae MYO2* gene encodes an essential myosin for vectorial transport of vesicles. J. Cell Biol. **113:**539–551.
18. **Kagami, M., A. Toh-e, and Y. Matsui.** 1997. *SRO9*, a multicopy suppressor of the bud growth defect in the *Saccharomyces cerevisiae rho3*-deficient cells, shows strong genetic interactions with tropomyosin genes, suggesting its role in organization of the actin cytoskeleton. Genetics **147:**1003–1016.

19. **Kaiser, C., S. Michaelis, and A. Mitchell.** 1994. Methods in yeast genetics. Cold Spring Harbor Laboratory Press, Cold Spring Harbor, N.Y.
20. **Lapierre, L. A., R. Kumar, C. M. Hales, J. Navarre, S. G. Bhartur, J. O. Burnette, D. W. Provance, Jr., J. A. Mercer, M. Bahler, and J. R. Goldenring.** 2001. Myosin-Vb is associated with plasma membrane recycling systems. Mol. Biol. Cell **12:**1843–1857.
21. **Lazar, T., M. Gotte, and D. Gallwitz.** 1997. Vesicular transport: how many Ypt/Rab-GTPases make a eukaryotic cell? Trends Biochem. Sci. **22:**468–472.
22. **Lazzarino, D. A., I. Boldogh, M. G. Smith, J. Rosand, and L. A. Pon.** 1994. Yeast mitochondria contain ATP-sensitive, reversible actin-binding activity. Mol. Biol. Cell **5:**807–818.
23. **Lillie, S. H., and S. S. Brown.** 1994. Immunofluorescence localization of the unconventional myosin, Myo2p, and the putative kinesin-related protein, Smy1p, to the same regions of polarized growth in *Saccharomyces cerevisiae*. J. Cell Biol. **125:**825–842.
24. **Matsui, Y., and A. Toh-e.** 1992. Yeast *RHO3* and *RHO4 ras* superfamily genes are necessary for bud growth, and their defect is suppressed by a high dose of bud formation genes *CDC42* and *BEM1*. Mol. Cell. Biol. **12:**5690–5699.
25. **Menasche, G., E. Pastural, J. Feldmann, S. Certain, F. Ersoy, S. Dupuis, N. Wulffraat, D. Bianchi, A. Fischer, F. Le Deist, and G. de Saint Basile.** 2000. Mutations in RAB27A cause Griscelli syndrome associated with haemophagocytic syndrome. Nat. Genet. **25:**173–176.
26. **Miyakawa, I., H. Aoi, N. Sando, and T. Kuroiwa.** 1984. Fluorescence microscopic studies of mitochondrial nucleoids during meiosis and sporulation in the yeast, *Saccharomyces cerevisiae.* J. Cell Sci. **66:**21–38.
27. **Morishita, T., and I. Uno.** 1991. A dominant interfering mutation (*CYR3*) of the *Saccharomyces cerevisiae RAS2* gene. J. Bacteriol. **173:**4533–4536.
28. **Morris, R. L., and P. J. Hollenbeck.** 1995. Axonal transport of mitochondria along microtubules and F-actin in living vertebrate neurons. J. Cell Biol. **131:**1315–1326.
29. **Prinz, W. A., L. Grzyb, M. Veenhuis, J. A. Kahana, P. A. Silver, and T. A. Rapoport.** 2000. Mutants affecting the structure of the cortical endoplasmic reticulum in *Saccharomyces cerevisiae.* J. Cell Biol. **150:**461–474.
30. **Provance, D. W., M. Wei, V. Ipe, and J. A. Mercer.** 1996. Cultured melanocytes from *dilute* mutant mice exhibit dendritic morphology and altered melanosome distribution. Proc. Natl. Acad. Sci. USA **93:**14554–14558.
31. **Rossanese, O. W., C. A. Reinke, B. J. Bevis, A. T. Hammond, I. B. Sears, J. O'Connor, and B. S. Glick.** 2001. A role for actin, Cdc1p, and Myo2p in the inheritance of late Golgi elements in *Saccharomyces cerevisiae.* J. Cell Biol. **153:**47–62.
32. **Schott, D., J. Ho, D. Pruyne, and A. Bretscher.** 1999. The COOH-terminal domain of Myo2p, a yeast myosin V, has a direct role in secretory vesicle targeting. J. Cell Biol. **147:**791–808.
33. **Sikorski, R. S., and P. Hieter.** 1989. A system of shuttle vectors and yeast host strains designed for efficient manipulation of DNA in *Saccharomyces cerevisiae.* Genetics **122:**19–27.
34. **Simon, V. R., S. L. Karmon, and L. A. Pon.** 1997. Mitochondrial inheritance: cell cycle and actin cable dependence of polarized mitochondrial movements in *Saccharomyces cerevisiae.* Cell Motil. Cytoskeleton **37:**199–210.
35. **Simon, V. R., T. C. Swayne, and L. A. Pon.** 1995. Actin-dependent mitochondrial motility in mitotic yeast and cell-free systems: identification of a motor activity on the mitochondrial surface. J. Cell Biol. **130:**345–354.
36. **Sturmer, K., O. Baumann, and B. Walz.** 1995. Actin-dependent light-induced translocation of mitochondria and ER cisternae in the photoreceptor cells of the locust *Schistocerca gregaria*. J. Cell Sci. **108:**2273–2283.
37. **Sutton A., D. Immanuel, and K. T. Arndt.** 1991. The SIT4 protein phosphatase functions in late G_1 for progression into S phase. Mol. Cell. Biol. **11:**2133–2148.
38. **Vida, T. A., and S. D. Emr.** 1995. A new vital stain for visualizing vacuolar membrane dynamics and endocytosis in yeast. J. Cell Biol. **128:**779–792.
39. **Wilson, S. M., R. Yip, D. A. Swing, T. N. O'Sullivan, Y. Zhang, E. K. Novak, R. T. Swank, L. B. Russell, N. G. Copeland, and N. A. Jenkins.** 2000. A mutation in Rab27a causes the vesicle transport defects observed in ashen mice. Proc. Natl. Acad. Sci. USA **97:**7933–7938.
40. **Wu, X., G. Jung, and J. A. Hammer.** 2000. Functions of unconventional myosins. Curr. Opin. Cell Biol. **12:**42–51.
41. **Wu, X., K. Rao, M. B. Bowers, N. G. Copeland, N. A. Jenkins, and J. A. Hammer III.** 2001. Rab27a enables myosin Va-dependent melanosome capture by recruiting the myosin to the organelle. J. Cell Sci. **114:**1091–1100.
42. **Wu, X. S., K. Rao, H. Zhang, F. Wang, J. R. Sellers, L. E. Matesic, N. G. Copeland, N. A. Jenkins, and J. A. Hammer III.** 2002. Identification of an organelle receptor for myosin-Va. Nat. Cell Biol. **4:**271–278.
43. **Yaffe, M. P.** 1999. The machinery of mitochondrial inheritance and behavior. Science **283:**1493–1497.
44. **Yin, H., D. Pruyne, T. C. Huffaker, and A. Bretscher.** 2000. Myosin V orientates the mitotic spindle in yeast. Nature **406:**1013–1015.
45. **Ziman, M., J. M. O'Brien, L. A. Ouellette, W. R. Church, and D. I. Johnson.** 1991. Mutational analysis of *CDC42Sc*, a *Saccharomyces cerevisiae* gene that encodes a putative GTP-binding protein involved in the control of cell polarity. Mol. Cell. Biol. **11:**3537–3544.